Susceptible host dynamics explain pathogen resilience

Sang Woo Park, . . . , Sarah Cobey

Abstract

Major priority for epidemiological research in the time of anthropogenic change is understanding how infectious disease dynamics respond to perturbations. Interventions to slow the spread of COVID-19 significantly disrupted the transmission of other human pathogens, providing unique opportunities to learn about pathogen characteristics from spatiotemporal variation in re-emergence patterns. As interventions lifted, a key question of whether and when respiratory pathogens would eventually return to their pre-pandemic dynamics remains to be answered. To address this gap, we develop a framework for estimating pathogen resilience based on how fast epidemic patterns return to their pre-pandemic, endemic cycles. Our analysis reveals a possibility that some pathogens may have settled to endemic cycles that are different from their pre-pandemic patterns. Finally, we show that heterogeneity in pathogen resilience can be understood in terms of how fast a susceptible host population becomes replenished. Our framework offers a novel perspective to characterizing epidemic dynamics of endemic pathogens and measuring epidemic time scales.

Understanding how ecological systems respond to perturbations is a fundamental challenge in predicting species persistence and extinction [1, 2, 3]. These responses can be characterized in terms of resilience, which often measures how fast a system returns to its stable, reference state following a perturbation [4, 5, 6, 7]. Both theoretical and empirical efforts to quantify resilience of ecological systems have provided key insights for understanding the dynamics of complex systems and linking these findings to actionable strategies for species conservation [8]. However, despite rich literature on ecological resilience, there have been limited applications to measuring the resilience of host-pathogen systems, especially for human pathogens.

Non-pharmaceutical interventions (NPIs) to slow the spread of COVID-19 disrupted the transmission of other human pathogens, providing large-scale natural experiments for understanding how various host-pathogen systems respond to perturbations [9, 10, 11, 12]. In particular, as interventions lifted, large heterogeneities in outbreak dynamics were observed across different pathogens in different countries (Figure 1), likely reflecting differences in NPI patterns, pathogen characteristics, immigration/importantion from other countries, and pre-pandemic pathogen dynamics [13]. Even though more than four years have already passed since the emergence of COVID-19, current circulation patterns for many respiratory pathogens appear to be different from their pre-pandemic, seasonal patterns, especially in Hong Kong and Korea: some pathogens, such as human metapneumovirus and bocavirus in Korea, are circulating at lower levels, whereas other pathogens, such as RSV in Korea, seem to exhibit different seasonality (Figure 1). These observations pose two fundamental questions for current and future infectious disease dynamics: (1) can we learn about underlying pathogen characteristics, such as their transmissibility or duration of immunity, from re-emergence patterns? and (2) can we predict whether and when other respiratory pathogens will eventually return to their pre-pandemic dynamics?

To address this question, we propose a framework for characterizing the resilience of a host-pathogen system based on how fast the system recovers from perturbation. We begin by laying out a few representative scenarios that capture the potential impact of COVID-19 interventions on endemic pathogen dynamics and illustrating how resilience can be measured by comparing the pre- and post-pandemic dynamics of susceptible and infected hosts. In practice, information on susceptible hosts are often unavailable, and traditional methods for reconstructing the dynamics of susceptible hosts require long-term endemic time series [14, 15], which cannot be applied due to disruptions in epidemic patterns caused by COVID-19 interventions. Instead, we utilize Takens' embedding theorem to reconstruct empirical attractors from data and further measure the distance from this empirical attractor [16]. This reconstruction allows us to characterize the rate at which this distance decreases over time, which correspond to pathogen resilience. We apply this framework to analyzing pathogen surveillence data for a wide array of respiratory and non-respiratory pathogens from Canada, Hong Kong, Korea, and US. Finally, we show that susceptible host dynamics are a key determinants of pathogen resilience. Our study offers unique insights into understanding pathogen re-emergence patterns following COVID-19 interventions.

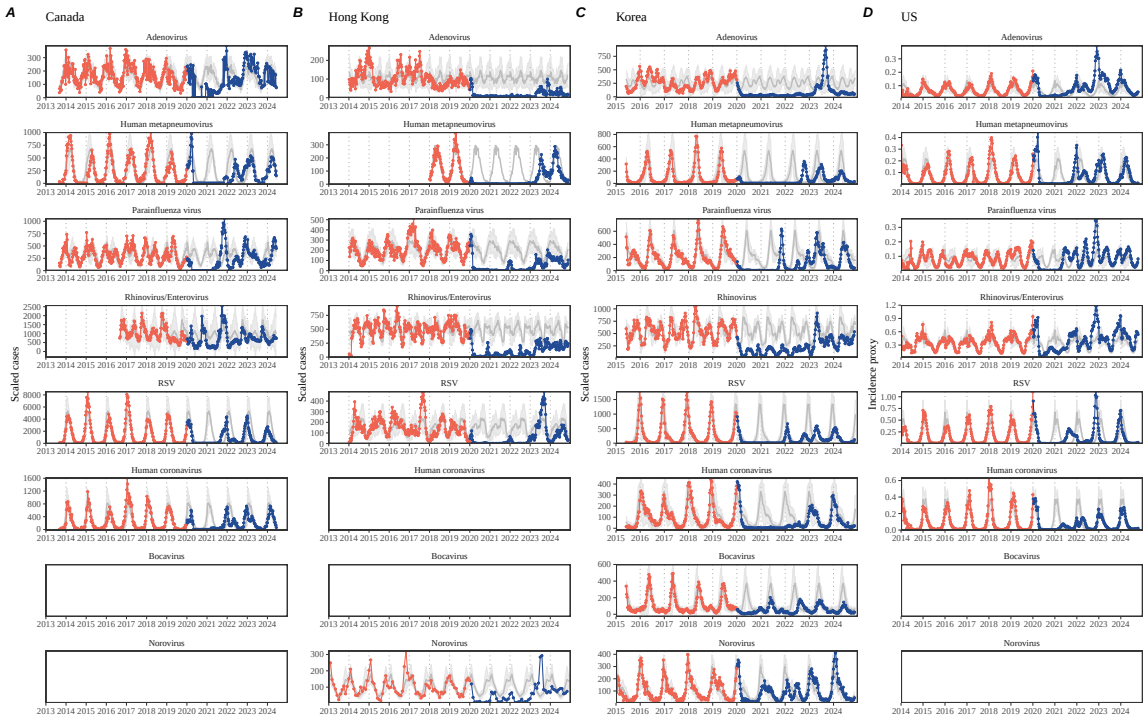

Figure 1: **Observed heterogeneity in responses to COVID-19 pandemic across respiratory pathogens and norovirus in (A) Canada, (B) Hong Kong, (C) Korea, and (D) US.** Red points and lines represent data before 2020. Blue points and lines represent data since 2020. Gray lines and shaded regions represent the mean seasonal patterns and corresponding 95% confidence intervals based on the observed outbreak patterns before 2020.

Conceptual introduction to pathogen resilience

In classical ecological literature, resilience of an ecological system is measured by the rate at which the system returns to its reference state following a perturbation [4, 5, 6, 7]. This rate corresponds to the largest real part of the eigenvalues of the linearized system near equilibrium—here, we refer to this value as the *intrinsic* resilience of the system, which represents the expected rate of return from perturbated states. However, respiratory pathogens often exhibit seasonal variation in transmission, meaning that the intrinsic resilience of a host-pathogen system varies across season. Nonetheless, we can still measure the *empirical* resilience of a host-pathogen system by looking at how fast the system returns to the pre-pandemic, endemic dynamics after interventions are lifted.

As an example, consider an intervention that reduce transmission by 50% for 6 months starting in 2020, which causes epidemic patterns to deviate from its original stable annual cycle for a short period of time and eventually come back (Figure 2A). To measure the empirical resilience of this system, we first need to be able to measure

the distance from its pre-pandemic attractor. There are many different ways we can measure the distance from attractor, but for illustrative purposes, we choose one of the most parsimonious approach: that is, we look at how the susceptible (S) and infected (I) populations change over time and measure the distance on the SI phase plane (Figure 2B). In this simple case, the locally estimated scatterplot smoothing (LOESS) fit indicates that the distance from attractor decreases linearly on average (Figure 2C). Furthermore, the overall rate of return matches the intrinsic resilience of the seasonally unforced system (Figure 2C).

Alternatively, NPIs can permanently change our behavior and have persisting impact on the pathogen dynamics; as an example, we consider a scenario in which a 10% reduction in transmission persists even after the NPIs are lifted (Figure 2D–F). In such cases, we cannot know whether the pathogen will return to its original cycle or a different cycle until many years have passed after the NPIs are lifted, meaning that we cannot measure the distance against the new attractor that the system will eventually approach. Nonetheless, we can still measure the distance against the original, pre-pandemic attractor and ask how the distance changes over time (Figure 2E). The LOESS fit suggests that the distance from the attractor will initially decrease exponentially on average (equivalently, linearly on a log scale) and eventually plateau (Figure 2F). Here, a permanent 10% reduction in transmission rate slows down the system, which causes the distance from the attractor to decrease at a slower rate (Figure 2F) than it would have otherwise in the absence of permanent transmission reduction (Figure 2C). This example shows that resilience is not necessarily an intrinsic property of a specific pathogen. Instead, pathogen resilience is a property of a specific attractor that a host-pathogen system approaches, which depends on both pathogen and host characteristics.

Finally, transient phenomena can also complicate the picture (Figure 2G–I). For example, a stage-structured model for RSV initially exhibits a stable annual cycle, but perturbations from NPIs cause the epidemic to exhibit biennial cycles (Figure 2G). Despite this biennial cycle, we see that the system eventually approaches the original pre-pandemic attractor (Figure 2H), suggesting that this biennial cycle is a transient phenomenon. The LOESS fit indicates that the distance from the attractor will initially decrease exponentially at a rate that is consistent with the intrinsic resilience of the seasonally unforced system, but the rate of decrease slows down as the epidemic exhibits a biennial cycle (Figure 2I). In classical ecological theory, this behavior is also referred to as a ghost attractor, which causes long transient dynamics and slow transitions [17]. As we show in Supplementary Figure S1, strong seasonal forcing in transmission can also lead to transient phenomena for a simple SIRS model, causing a slowing down of the system.

In Supplementary Materials, we also explore measuring the resilience of a two-strain host-pathogen system: when the dynamics two strains (or two pathogens) are coupled through cross immunity, we would expect the entire system to be characterized by a single resilience value (rather than having two separate resilience for each strain). Simulations from a simple two-strain system illustrate that separate anal-

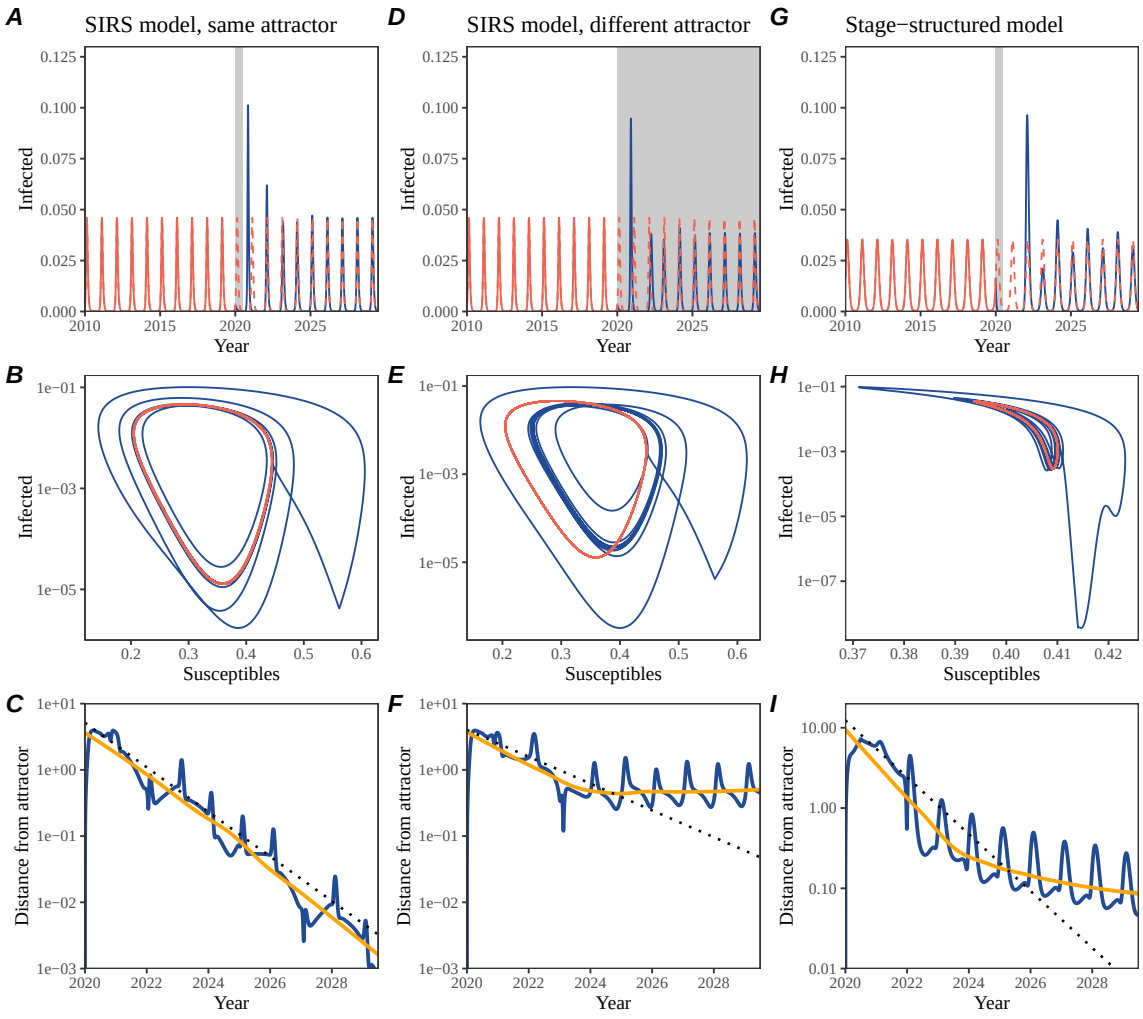

Figure 2: **Conceptual framework for measuring pathogen resilience following NPIs across different scenarios.** (A, D, G) Simulated epidemic trajectories across various models. Red and blue solid lines represent epidemic dynamics before and after interventions are introduced, respectively. Red dashed lines represent counterfactual epidemic dynamics in the absence of interventions. Gray regions indicate the duration of interventions. (B, E, H) Phase plane representation of the corresponding model. Red and blue solid lines represent epidemic trajectories on an SI phase plane before and after interventions are introduced, respectively. (C, F, I) Changes in logged distance from attractor over time. Blue lines represent the logged distance from attractor. Orange lines represent the locally estimated scatterplot smoothing (LOESS) fits to the logged distance from attractor. Dotted lines are superimposed as a comparison to have the same slope as the intrinsic resilience of the seasonally unforced system.

yses of individual strain dynamics (e.g., RSV A vs B) and a joint analysis of total

infections (e.g., total RSV infections) yield identiacl resilience estimates, confirming our expectation (Supplementary Figure S2, 3). Analogous to a single system, strong seasonal forcing in transmission can cause the system to slow down through transient phenomena (Supplementary Figure S4).

These observations indicate three possibilities. First, we can directly estimate the empirical resilience of a host-pathogen system by looking at how fast the system approaches a pre-pandemic attractor, provided that we can measure the distance from attractor. The empirical approach to estimating pathogen resilience is particularly convenient because it does not require us to know the true underlying model. As we show in Supplementary Figure S5, estimating the intrinsic resilience from fitting standard compartmental models can lead to biased estimates, especially under model misspecification. Second, resilience estimates allow us to make phenomenological predictions about the dynamics of a host-pathogen system following a perturbation: assuming that the distance from the attractor will decrease exponentially over time, we can obtain a ballpark estimate for when the system will reach an attractor. Finally, deviation from an exponential decrease in the distance from attractor can provide information about whether the system has reached an alternative attractor, or a ghost attractor, that is different from the original, pre-pandemic attractor. These alternative attractors may reflect continued perturbations from permanent changes in transmission patterns as well as changes in immune landscapes.

Inferring pathogen resilience from real data

Based on these observations, we now set out to infer pathogen resilience from real data. Here, we briefly lay out our approach to estimating pathogen resilience from real data (Figure 3). We then test this approach against simulations and apply it to real data.

So far, we focused on simple examples that assume a constant transmission reduction. However, in practice, the impact of NPIs on pathogen transmission is likely more complex (Figure 3A), reflecting introduction and relaxation of various intervention strategies. These complexities can lead to longer delays between the introduction of NPIs and pathogen re-emergence as well as temporal variation in outbreak sizes (Figure 3B): in this example, continued transmission reduction from NPIs limits the size of the first outbreak in 2021 following the emergence, allowing for a larger outbreak in 2022 when NPIs are further relaxed.

Previously, we relied on the dynamics of susceptible and infected hosts to compute the distance from attractor (Figure 2), but information on susceptible hosts are often not available in practice. In addition, uncertainties in case counts due to observation error as well as the possibility of complex, multiannual attractor adds challenges to measuring the distance from attractor. To address these challenges, we first reconstruct an empirical attractor by utilizing Takens' theorem, which states that an attractor of a nonlinear multidimensional system can be mapped onto a

delayed embedding [16]. Here, we use delayed copies of logged values of pre-pandemic cases $C(t)$ (Figure 3C) to reconstruct the attractor:

$$\langle \log(C(t)+1), \log(C(t-\tau)+1), \ldots, \log(C(t-(M-1)\tau)+1) \rangle, \tag{1}$$

where the delay τ and embedding dimension M are determined based on autocorrelations and false nearest neighbors, respecitvely [18, 19]. We then apply the same delay and embedding dimensions to the entire time series to determine the position on a multi-dimensional state space (Figure 3D), which allows us to measure the nearest neighbor distance between the current state of the system and the empirical attractor (Figure 3E). In principle, we can quantify how fast this distance decreases by fitting a linear regression on a log scale, where the slope of the linear regression corresponds to pathogen resilience. As we show in Supplementary Figure S6, overall temporal variations in the distance from attractor, especially the observed rate of decrease, appear robust to choices about embedding delays and diemsions; we note that using longer delays and higher dimensions tend to smooth out temporal variations in the distance from attractor.

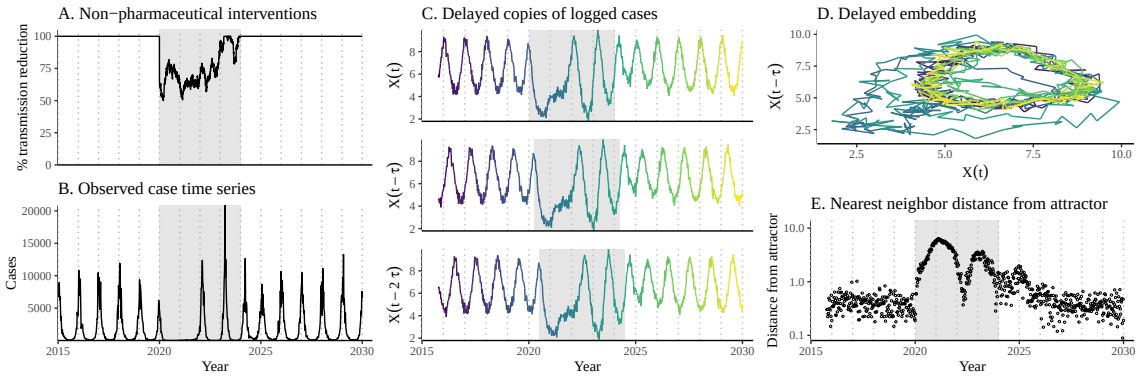

Figure 3: **A schematic diagram explaining how pathogen resilience can be inferred from real data.** (A) A realistic example of a synthetic NPI, represented by a relative reduction in transmission. (B) The impact of the synthetic NPI on epidemic dynamics simulated using a stochastic SIRS model. (C) Generating delayed copies of the logged time series allows us to obtain an embedding. (D) Two dimensional representation of an embedding. (E) Delayed embedding allows us to calculate the nearest neighbor distance from the empirical attractor, which is determined based on the pre-pandemic time series. This distance time series can be used to infer pathogen resilience by fitting a linear regression after choosing an appropriate window for regression.

Complex changes in the distance from attractor suggest that estimating pathogen resilience from linear regression will likely be sensitive to our choice of fitting windows for the regression. In Supplementary Materials, we explore an automated window selection criteria for linear regression and test it against randomized, stochastic simulations across a wide range of realistic NPI shapes. We find that resilience estimates

based on the automated window selection criteria are moderately correlated (0.54) with the intrinsic resilience of the post-NPI attractor. In contrast, a naive approach that uses the entire time series, starting from the peak distance, only gives a correlation of 0.21 and consistently underestimates the intrinsic resilience.

Now, we apply this approach to pathogen surveillance data presented in Figure 1. For each time series, we apply Takens' theorem independently to reconstruct the empirical attractor and obtain the corresponding time series of distance from attractors ([**SWP:** *Supp*]). Then, we use the automated window selection criteria to fit a linear regression and estimate the empirical resilience for each pathogen in each country. For most respiratory pathogens, resilience estimates 0.5/year and 2/year (Figure 4A), with the exception of Rhinovirus in the US (0.066/year; 95% CI: 0.018/year–0.113/year) and Bocavirus in Korea (0.087/year; 95% CI: 0.023/year–0.151/year). Excluding these exceptions, the mean resilience of common respiratory pathogens is 0.974/year (95% CI: 0.784/year–1.16/year). As a reference, this is ≈ 7 times higher than the intrinsic resilience of pre-vaccination measles dynamics (≈ 0.13/year). Finally, resilence estimates for norovirus appears to be comparable to the intrinsic resilience of measles: 0.119/year (95%CI: 0.004/year–0.233/year) for Korea and 0.385/year (95% CI: 0.167/year–0.603/year). A simple ANOVA shows that there are significant differences in resilience estimates across countries ($p < 0.036$) and pathogens ($p < 0.030$).

Using resilience estimates, we now predict when each pathogen will return to their original pre-pandemic cycles. Specifically, we extend our linear regression fits to distance-from-attractor time series and ask when the predicted regression line will cross a threshold value, which we set to a mean of pre-pandemic distances. We predict that a return to pre-pandemic cycles would be imminent for most pathogens (Figure 4B). In addition, we also predict that many pathogens should have already returned to their pre-pandemic dynamics by the end of 2024; but these predictions contradict some of the observed pathogen dynaics. For example, we predict that both human metapneumovirus and RSV in Korea should have returned to their attractors by now, but the magnitude and timing of recent epidemics are different from pre-pandemic patterns (Figure 1). These observations suggest the possibility that some common respiratory pathogens may have converged to different attractors.

Susceptible host dynamics explain variation in pathogen resilience

So far, we focused on quantifying pathogen resilience from the observed patterns of pathogen re-emergence following COVID-19 interventions. But what factors determine how resilient a host-pathogen system is? Here, we use a standard Susceptible-Infected-Recovered-Susceptible (SIRS) model to show that susceptible host dynamics are the key determinants of pathogen resilience. To do so, we vary the basic reproduction number $\mathcal{R}_0$, which represents the average number of secondary infections caused

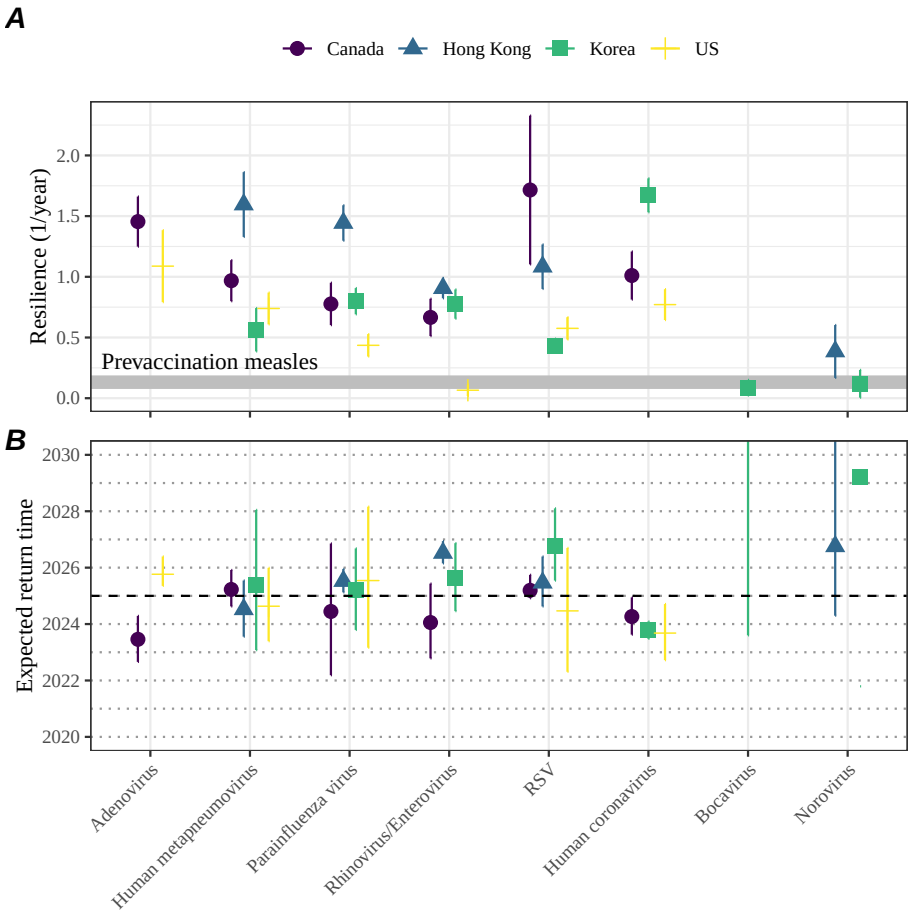

Figure 4: **Summary of resilience estimates.** (A) Estimated pathogen resilience. The gray horizontal line represents the intrinsic resilience of pre-vaccination measles dynamics. (B) Predicted timing of when each pathogen will return to their pre-pandemic cycles. The dashed line in panel B indicates the end of 2024 (current observation time). Error bars represent 95% confidence intervals.

by a newly infected individual in a fully susceptible population, and the duration of immunity and compute intrinsic resilience for each parameter.

We find an increase in $\mathcal{R}_0$ and a decrease in duration of immunity correspond to an increase in pathogen resilience (Figure 5A). These variations can be understood in terms of the susceptible host dynamics, where faster per-capita susceptible replenishment rate causes the system to be more resilient (Figure 5B). This rate can be expressed as a ratio between absolute rate at which new susceptibles enter the population and the equilibrium number of susceptible individuals in the population, $\bar{S}$. Therefore, both higher $\mathcal{R}_0$ and shorter duration of immunity can drive faster per-capita susceptible replenishment rate (Figure 5B), especially because higher $\mathcal{R}_0$ leads to lower $\bar{S}$.

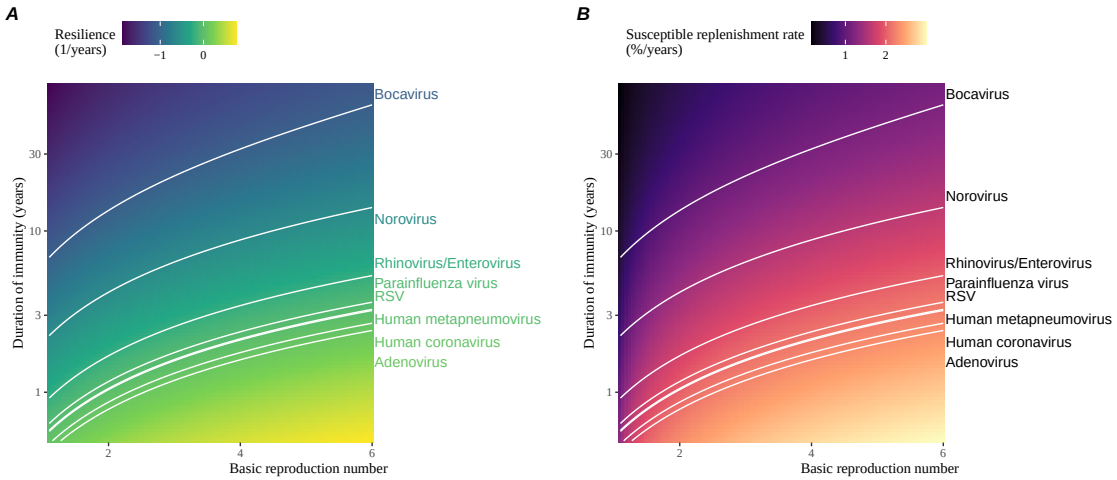

Figure 5: **Linking pathogen resilience to epidemiological parameters and susceptible host dynamics.** (A) The heat map represents intrinsic resilience as a function of the basic reproduction number $\mathcal{R}_0$ and the duration of immunity. (B) The heat map represents per-capita susceptible replenishment rate as a function of the basic reproduction number $\mathcal{R}_0$ and the duration of immunity. The standard SIRS model is used to compute intrinsic resilience and per-capita susceptible replenishment rate. Lines correspond to a set of parameters that are consistent with mean resilience estimates for each pathogen. Pathogens are ranked based on their mean resilience estimates, averaged across different countries.

Finally, we can now rank different pathogens based on the average values of empirical resilience, which allows us to determine a set of parameters that are consistent with the estimated resilience (Figure 5A). Across all pathogens we consider, except for bocavirus and norovirus, we estimate that the average duration of immunity is likely to be short (< 6 years) across a plausible range of $\mathcal{R}_0$. These rankings further allow us to map each pathogen onto a set of parameters that are consistent with its empirical resilience (Figure 5A) and obtain a plausible range of susceptible replenishment rates for each pathogen (Figure 5B). However, we note that there is no one-to-one correspondance between susceptible replenishment rates and pathogen resilience, leading to a wide uncertainty in the estimates for susceptible replenishment rates (Figure 5B).

Discussion

The COVID-19 interventions have caused major disruptions to circulation patterns of both respiratory and non-respiratory pathogens, adding challenges to predicting their future dynamics. On the other hand, these interventions offer large-scale natural experiments for understanding how different pathogens respond to perturbations. In

this study, we show that pathogen re-emergence patterns following COVID-19 interventions can be characterized through the lens of ecological resilience. Traditionally, ecological resilience measures how fast a system returns to a reference state following a perturbation. In the context of respiratory pathogens, resilience measures how fast epidemics return to their endemic cycles after interventions are lifted.

We use an attractor reconstruction approach to quantify how distance from attractor changes over time for each pathogen. By fitting a linear regression to log distances, we can estimate pathogen resilience and further predict when each pathogen will return to their endemic cycles. Consistency in resilience estimates across countries is particularly surprising given that each country imposed different intervention measures; this consistency provides robustness to our estimates. The ability to predict future epidemic patterns from resilience estimates also offers a new paradigm for epidemic forecasting. While this approach cannot predict the exact timing of outbreaks or epidemic patterns, it is nonetheless useful for predicting when epidemics will settle down to regular cycles after a large perturbation, such as COVID-19 interventions.

Our analyses suggest a possibility that several pathogens may have converged to different endemic cycles compared to their pre-pandemic epidemic patterns. Key examples include human metapnuemovirus, RSV, and bocavirus in Korea as well as RSV in Hong Kong. These changes may reflect permanent changes in behavior since 2020 or a shift in population-level immunity. However, it seems unlikely that permanent changes in behavior would only affect a few pathogens and not others. A shift in population-level immunity is plausible, as the emergence of SARS-CoV-2 and extinction of influenza B/Yamagata likely caused major changes in immune landscapes; however, we currently do not know how immunity, or lack thereof, from these pathogens would affect infection from other pathogens. Future studies should use detailed mechanistic models, coupled with behavioral and immunological data, to test these hypotheses and better understand post-pandemic dynamics of endemic pathogens.

We show that susceptible host dynamics shape pathogen resilience, where faster replenishment of the susceptible population causes the pathogen to be more resilient. For simplicity, we focus on waning immunity and birth as a main driver of the susceptible host dynamics but other mechanisms can also contribute to the replenishment of the susceptible population. In particular, pathogen evolution, especially the emergence of antigenically novel strains, can cause effective waning of immunity in the population; therefore, we tentatively hypothesize that faster rates of antigenic evolution can also cause a pathogen to be more resilient. Future studies should explore the relationship between the rate of evolution and resilience for antigenically evolving pathogens.

Quantifying pathogen resilience also offers novel approaches to validating epidemiological models. So far, the majority of model validation in epidemiology is based on the ability of a model to reproduce the observed epidemic dynamics and to predict future dynamics. However, there can be plethora of models that meet these

criteria. For example, two major RSV models have been proposed so far to explain biennial epidemic patterns: (1) a stage- and age-structured model that allows for disease severity to vary with number of past infections and age of infection and (2) a pathogen-interaction model that accounts for cross immunity between RSV and human metapnuemovirus. Since both models can accurately reproduce the observed epidemic patterns, standard criteria for model validation do not allow us to distinguish between these two models. Instead, we can measure the empirical resilience of each model by simulating various perturbations and compare them to estimates of empirical resilience from data, using COVID-19 interventions as an opportunity. Future studies should further investigate using pathogen resilience for validating epidemic models.

There are several limitations to our work. In particular, our estimates of pathogen resilience and the associated ranking are necessarily crude. [**SWP:** *Limitation TBD.*] Nonetheless, our study illustrates the utility of quantifying pathogen resilience for understanding how different pathogens respond to perturbations.

[**SWP:** *Conclusion paragraph TBD.*]

Materials and Methods

Data

We gathered time series on respiratory infections from four different countries: Canada, Hong Kong, Korea, and United States (US). As a reference, we also included time series data on norovirus infections for available countries—in contrast to respiratory pathogens, we expect gastrointestinal viruses, such as norovirus, to be less affected by COVID-19 intervention measures.

Weekly time series of respiratory infection cases in Canada come from the Respiratory Virus Detection Surveillance System, which collect data from select laboratories across Canada. We extracted the data from `https://www.canada.ca/en/public-health/services/surveillance/respiratory-virus-detections-canada.html`.

Weekly time series of respiratory infection cases in Hong Kong came from the Centre for Health Protection, Department of Health. We extracted the data from `https://www.chp.gov.hk/en/statistics/data/10/641/642/2274.html`.

Weekly time series of respiratory infection cases in Korea came from Korea Disease Control and Prevention Agency. We extracted the data from `https://dportal.kdca.go.kr/pot/is/st/ari.do`.

Finally, weekly time series of respiratory infection cases in the US comes from the National Respiratory and Enteric Virus Surveillance System.

Empirical attractor reconstruction

Linear regression

Mathematical modeling

Throughout the paper, we use a series of mathematical models to illustrate the concept of pathogen resilience and to understand the determinants of pathogen resilience. In general, the intrinsic resilience for a given system is given by the largest real part of the eigenvalues of the lineared system at endemic equilibrium. Here, we focus on the SIRS model and present the details of other models in Supplementary Materials. The SIRS (Susceptible-Infected-Recovered-Susceptible) model is the simplest model that allows for waning of immunity, where recovered (immune) individuals are assumed to become fully susceptible after an average of $1/\delta$ time period. The dynamics of the SIRS model is described by the following set of differential equations:

$$\frac{\mathrm{d}S}{\mathrm{d}t} = \mu - \beta(t)SI - \mu S + \delta R \tag{2}$$

$$\frac{\mathrm{d}I}{\mathrm{d}t} = \beta(t)SI - (\gamma + \mu)I \tag{3}$$

$$\frac{\mathrm{d}R}{\mathrm{d}t} = \gamma I - (\delta + \mu)R \tag{4}$$

$$\tag{5}$$

where μ represents the birth/death rate, $\beta(t)$ represents the time-varying transmission rate, and γ represents the recovery rate. The basic reprodcution number $\mathcal{R}_0 = \beta(t)/(\gamma + \mu)$ is defined as the average number of secondary infections caused by a single infected individual in a fully susceptible population and measures the intrinsic transmissibility of a pathogen.

For this model, the intrinsic resilience corresponds to:

$$-\frac{\mathrm{Re}(\lambda)}{2} = \frac{\delta + \beta I^* + \mu}{2}. \tag{6}$$

Here, I^* represents the prevalence values at endemic equilibrium:

$$I^* = \frac{(\delta + \mu)(\beta - (\gamma + \mu))}{\beta(\delta + \gamma + \mu)}. \tag{7}$$

The susceptible replenishment rate is given by:

$$S_{\text{replenish}} = \frac{\mu + \delta R}{S^*}, \tag{8}$$

where $S^* = 1/\mathcal{R}_0$ represents the equilibrium proportion of susceptible individuals.

When infection provides life-long immunity ($\delta \to 0$), the SIRS model becomes the SIR model. In this case, the intrinsic resilience is inversely proportional to the

In illustrating the impact of

Supplementary Text

Supplementary Figures

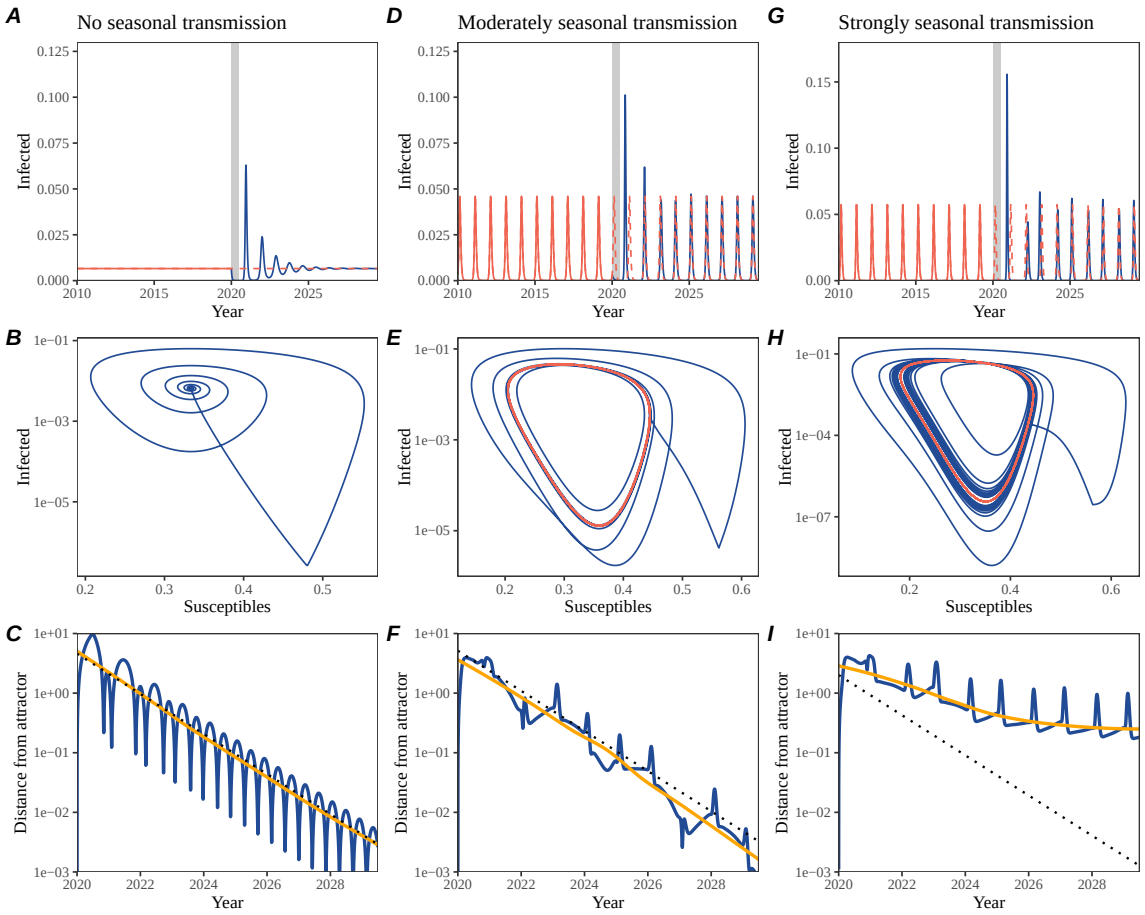

Figure S1: **Impact of seasonal transmission on pathogen resilience.** (A, D, G) Simulated epidemic trajectories using the SIRS model without seasonal forcing (A), with seasonal forcing of amplitude of 0.2 (D), and with seasonal forcing of amplitude of 0.2 (G). Red and blue solid lines represent epidemic dynamics before and after interventions are introduced, respectively. Red dashed lines represent counterfactual epidemic dynamics in the absence of interventions. Gray regions indicate the duration of interventions. (B, E, H) Phase plane representation of the corresponding model. Red and blue solid lines represent epidemic trajectories on an SI phase plane before and after interventions are introduced, respectively. (C, F, I) Changes in logged distance from attractor over time. Blue lines represent the logged distance from attractor. Orange lines represent the locally estimated scatterplot smoothing (LOESS) fits to the logged distance from attractor. Dotted lines are superimposed as a comparison to have the same slope as the intrinsic resilience of the seasonally unforced system.

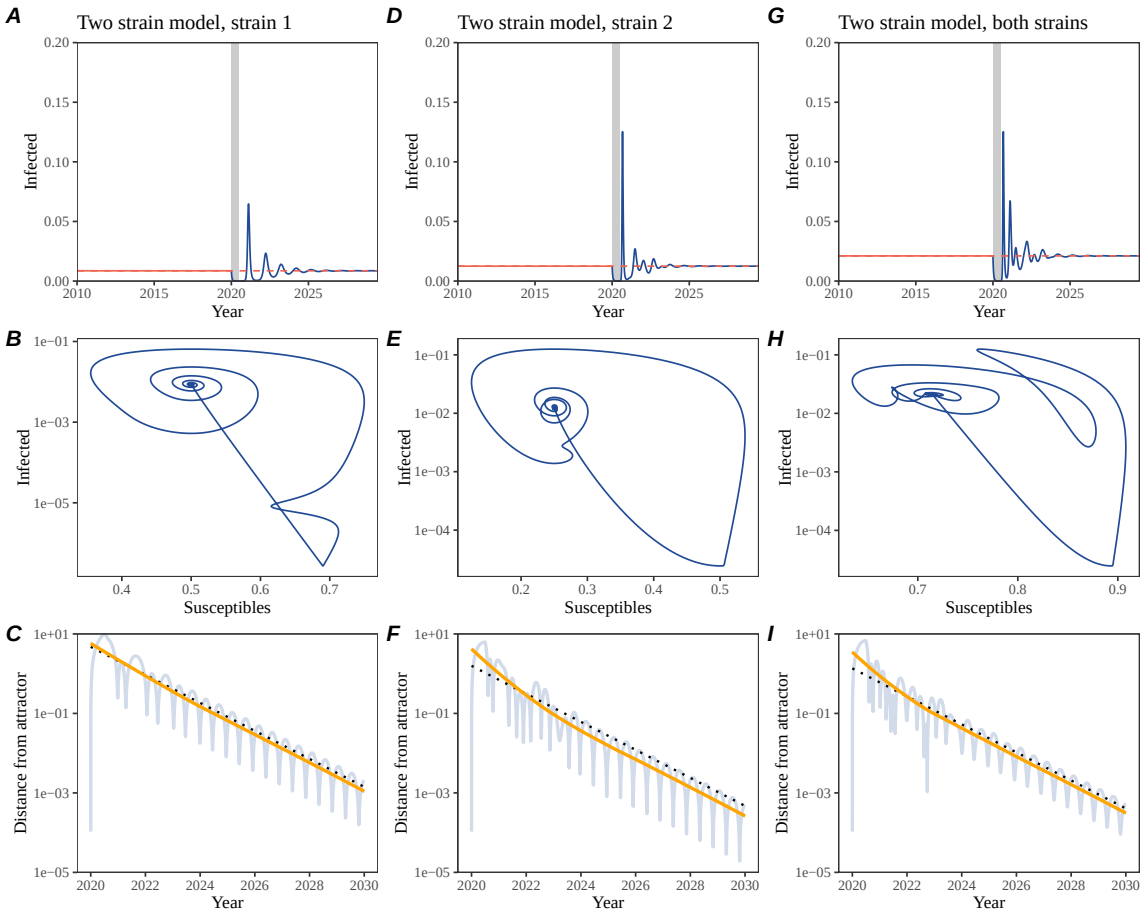

Figure S2: **Conceptual framework for measuring pathogen resilience following NPIs for a multi-strain system without seasonal forcing.** (A, D, G) Simulated epidemic trajectories using a multi-strain system without seasonal forcing. Red and blue solid lines represent epidemic dynamics before and after interventions are introduced, respectively. Red dashed lines represent counterfactual epidemic dynamics in the absence of interventions. Gray regions indicate the duration of interventions. (B, E, H) Phase plane representation of the corresponding model. Red and blue solid lines represent epidemic trajectories on an SI phase plane before and after interventions are introduced, respectively. (C, F, I) Changes in logged distance from attractor over time. Blue lines represent the logged distance from attractor. Orange lines represent the locally estimated scatterplot smoothing (LOESS) fits to the logged distance from attractor. Dotted lines are superimposed as a comparison to have the same slope as the intrinsic resilience of the seasonally unforced system.

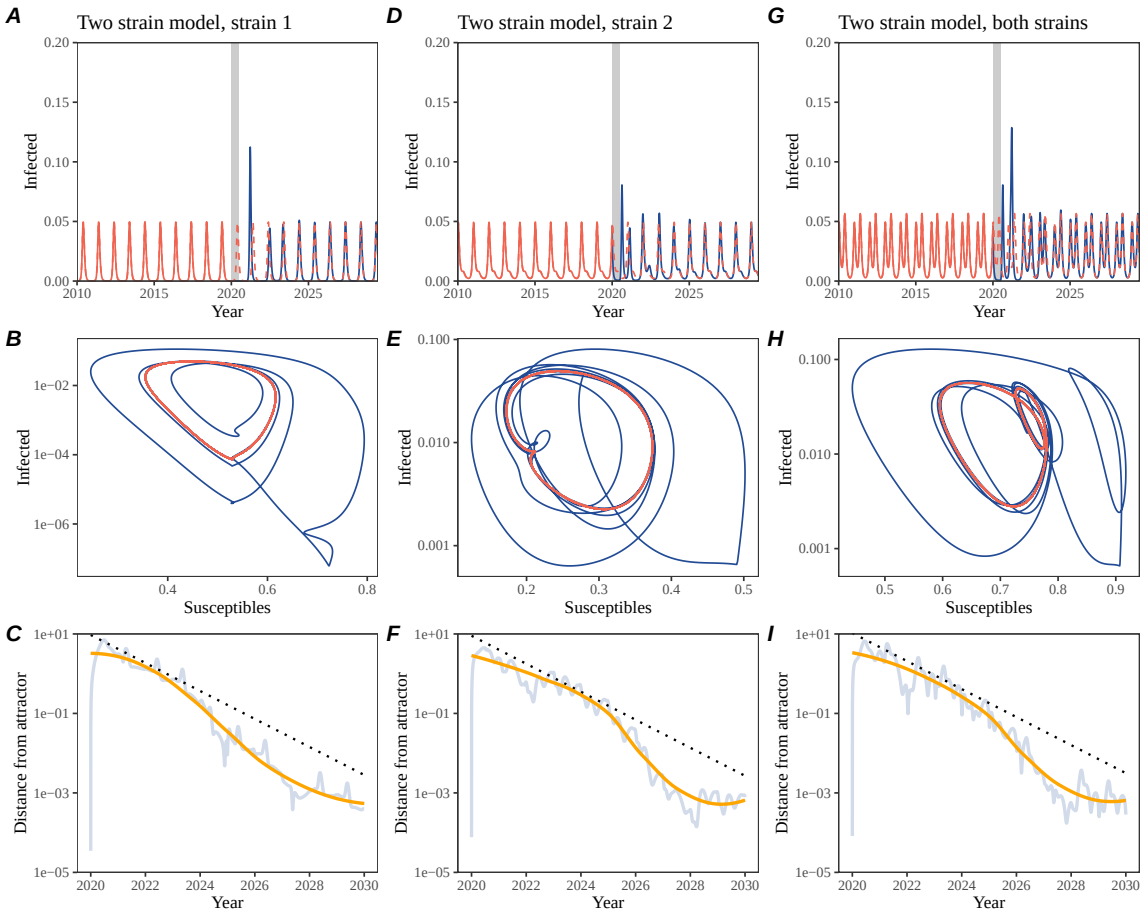

Figure S3: **Conceptual framework for measuring pathogen resilience following NPIs for a multi-strain system with seasonal forcing.** (A, D, G) Simulated epidemic trajectories using a multi-strain system with seasonal forcing (amplitude of 0.2). Red and blue solid lines represent epidemic dynamics before and after interventions are introduced, respectively. Red dashed lines represent counterfactual epidemic dynamics in the absence of interventions. Gray regions indicate the duration of interventions. (B, E, H) Phase plane representation of the corresponding model. Red and blue solid lines represent epidemic trajectories on an SI phase plane before and after interventions are introduced, respectively. (C, F, I) Changes in logged distance from attractor over time. Blue lines represent the logged distance from attractor. Orange lines represent the locally estimated scatterplot smoothing (LOESS) fits to the logged distance from attractor. Dotted lines are superimposed as a comparison to have the same slope as the intrinsic resilience of the seasonally unforced system.

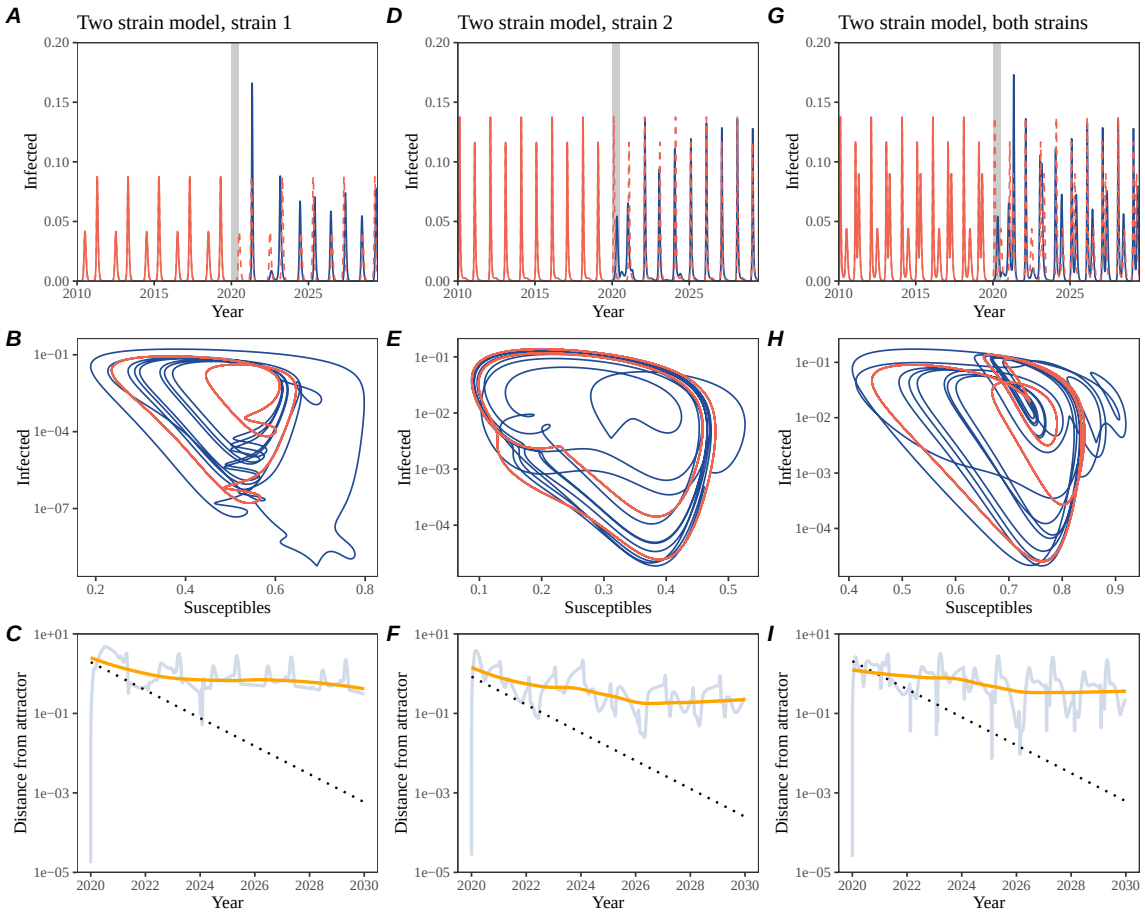

Figure S4: **Conceptual framework for measuring pathogen resilience following NPIs for a multi-strain system with strong seasonal forcing.** (A, D, G) Simulated epidemic trajectories using a multi-strain system with seasonal forcing (amplitude of 0.4). Red and blue solid lines represent epidemic dynamics before and after interventions are introduced, respectively. Red dashed lines represent counterfactual epidemic dynamics in the absence of interventions. Gray regions indicate the duration of interventions. (B, E, H) Phase plane representation of the corresponding model. Red and blue solid lines represent epidemic trajectories on an SI phase plane before and after interventions are introduced, respectively. (C, F, I) Changes in logged distance from attractor over time. Blue lines represent the logged distance from attractor. Orange lines represent the locally estimated scatterplot smoothing (LOESS) fits to the logged distance from attractor. Dotted lines are superimposed as a comparison to have the same slope as the intrinsic resilience of the seasonally unforced system.

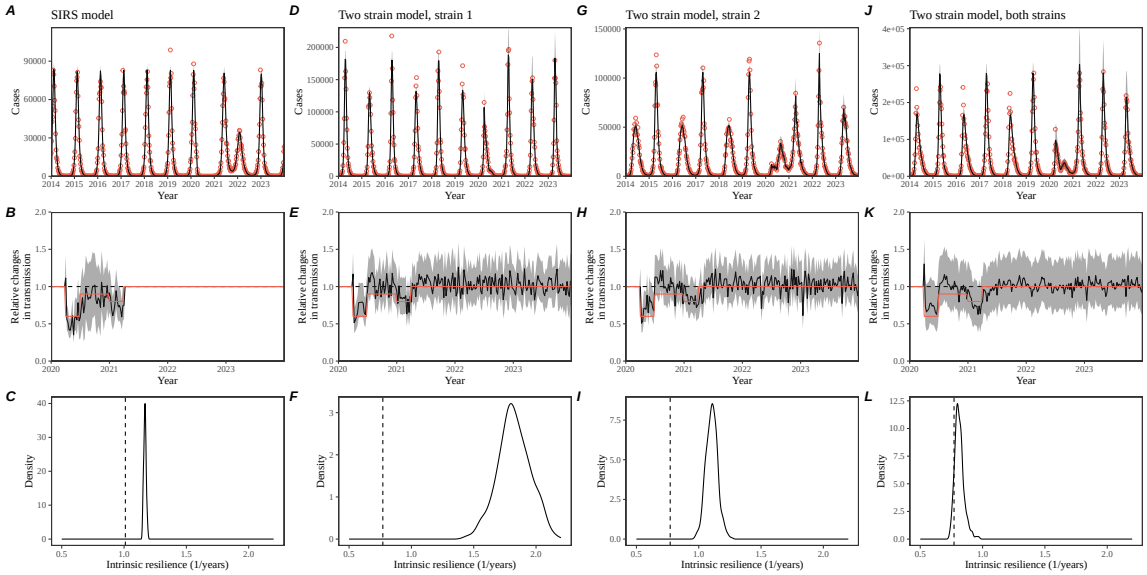

Figure S5: **Mechanistic model fits to simulated data and inferred intrinsic resilience.** (A, D, G, J) Simulated case time series from corresponding models (red) and SIRS model fits (black). (B, E, H, K) Assumed changes in transmission due to COVID-19 interventions (red) and estimated changes from the SIRS model (black). Solid lines and shaded regions represent fitted posterior median and 95% credible intervals. (C, F, I, L) True intrinsic reslience of the seasonally unforced system (vertical lines) and the posterior distribution of the inferred intrinsic resilience from the SIRS model (density plots).

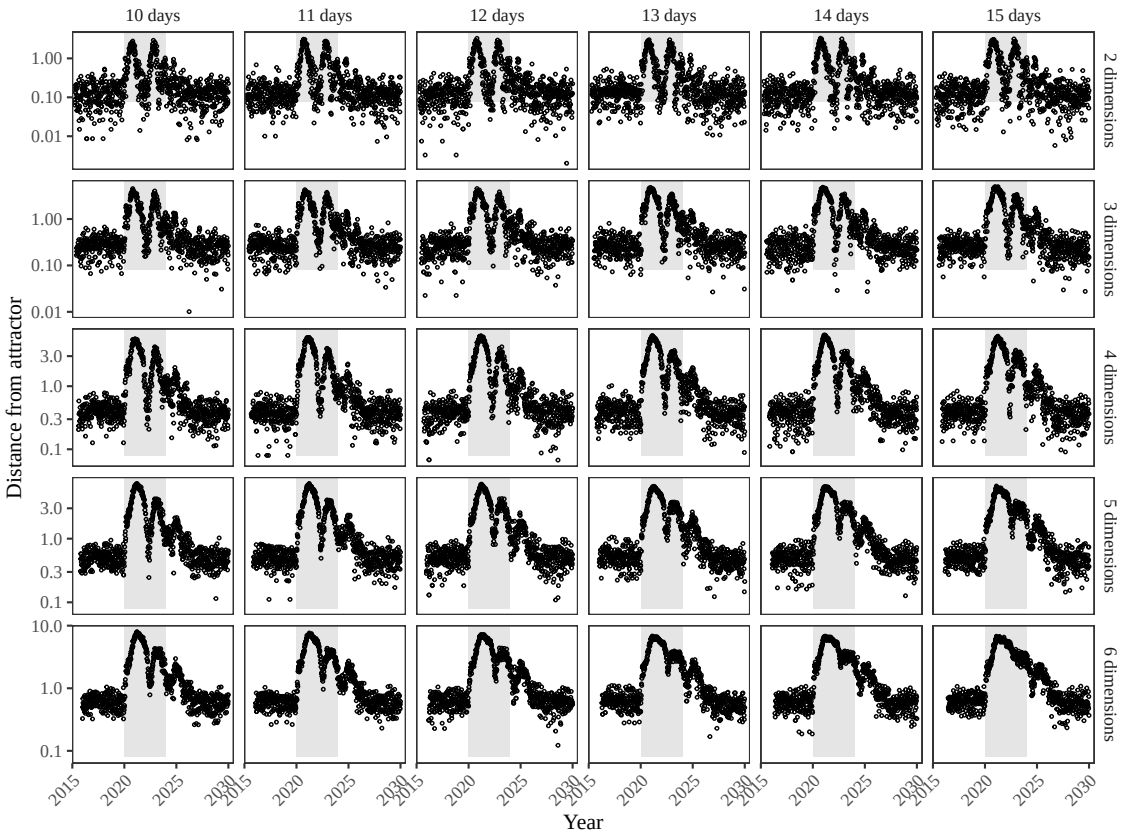

Figure S6: **Sensitivity of the distance from attractor to choices about emedding lags and dimensions.** Sensitivity analysis for the distance-from-attractor time series shown in Figure 3E in the main text by varying the embedding lag between 10–15 days and embedding dimensions between 2–6 dimensions.

References

[1] Edward A Bender, Ted J Case, and Michael E Gilpin. Perturbation experiments in community ecology: theory and practice. *Ecology*, 65(1):1–13, 1984.

[2] Anthony R Ives and Stephen R Carpenter. Stability and diversity of ecosystems. *science*, 317(5834):58–62, 2007.

[3] Marten Scheffer, Jordi Bascompte, William A Brock, Victor Brovkin, Stephen R Carpenter, Vasilis Dakos, Hermann Held, Egbert H Van Nes, Max Rietkerk, and George Sugihara. Early-warning signals for critical transitions. *Nature*, 461(7260):53–59, 2009.

[4] Stuart L Pimm. The structure of food webs. *Theoretical population biology*, 16(2):144–158, 1979.

[5] Michael G Neubert and Hal Caswell. Alternatives to resilience for measuring the responses of ecological systems to perturbations. *Ecology*, 78(3):653–665, 1997.

[6] Lance H Gunderson. Ecological resilience—in theory and application. *Annual review of ecology and systematics*, 31(1):425–439, 2000.

[7] Vasilis Dakos and Sonia Kéfi. Ecological resilience: what to measure and how. *Environmental Research Letters*, 17(4):043003, 2022.

[8] Jeanne C Chambers, Craig R Allen, and Samuel A Cushman. Operationalizing ecological resilience concepts for managing species and ecosystems at risk. *Frontiers in Ecology and Evolution*, 7:241, 2019.

[9] Rachel E Baker, Sang Woo Park, Wenchang Yang, Gabriel A Vecchi, C Jessica E Metcalf, and Bryan T Grenfell. The impact of COVID-19 nonpharmaceutical interventions on the future dynamics of endemic infections. *Proceedings of the National Academy of Sciences*, 117(48):30547–30553, 2020.

[10] Gabriela B Gomez, Cedric Mahé, and Sandra S Chaves. Uncertain effects of the pandemic on respiratory viruses. *Science*, 372(6546):1043–1044, 2021.

[11] Mihaly Koltai, Fabienne Krauer, David Hodgson, Edwin van Leeuwen, Marina Treskova-Schwarzbach, Mark Jit, and Stefan Flasche. Determinants of RSV epidemiology following suppression through pandemic contact restrictions. *Epidemics*, 40:100614, 2022.

[12] Sang Woo Park, Brooklyn Noble, Emily Howerton, Bjarke F Nielsen, Sarah Lentz, Lilliam Ambroggio, Samuel Dominguez, Kevin Messacar, and Bryan T Grenfell. Predicting the impact of non-pharmaceutical interventions against COVID-19 on Mycoplasma pneumoniae in the United States. *Epidemics*, 49:100808, 2024.

[13] Eric J Chow, Timothy M Uyeki, and Helen Y Chu. The effects of the COVID-19 pandemic on community respiratory virus activity. *Nature Reviews Microbiology*, 21(3):195–210, 2023.

[14] Georgiy V Bobashev, Stephen P Ellner, Douglas W Nychka, and Bryan T Grenfell. Reconstructing susceptible and recruitment dynamics from measles epidemic data. *Mathematical Population Studies*, 8(1):1–29, 2000.

[15] Bärbel F Finkenstädt and Bryan T Grenfell. Time series modelling of childhood diseases: a dynamical systems approach. *Journal of the Royal Statistical Society Series C: Applied Statistics*, 49(2):187–205, 2000.

[16] Floris Takens. Detecting strange attractors in turbulence. In *Dynamical Systems and Turbulence, Warwick 1980: proceedings of a symposium held at the University of Warwick 1979/80*, pages 366–381. Springer, 2006.

[17] Alan Hastings, Karen C Abbott, Kim Cuddington, Tessa Francis, Gabriel Gellner, Ying-Cheng Lai, Andrew Morozov, Sergei Petrovskii, Katherine Scranton, and Mary Lou Zeeman. Transient phenomena in ecology. *Science*, 361(6406):eaat6412, 2018.

[18] Matthew B Kennel, Reggie Brown, and Henry DI Abarbanel. Determining embedding dimension for phase-space reconstruction using a geometrical construction. *Physical review A*, 45(6):3403, 1992.

[19] Eugene Tan, Shannon Algar, Débora Corrêa, Michael Small, Thomas Stemler, and David Walker. Selecting embedding delays: An overview of embedding techniques and a new method using persistent homology. *Chaos: An Interdisciplinary Journal of Nonlinear Science*, 33(3), 2023.